NANO LETTERS

pubs.acs.org/NanoLett

Letter

Modulation of Single Photon Emission from Suspended 1L WSe_2 under Electrostatically Induced Strain

Frances Camille M. Wu, Shang-Hsuan Wu, Bin Fang, Xintong Li, Jadon Zheng, Jean Anne C. Incorvia, and Edward T. Yu*

Cite This: *Nano Lett.* 2025, 25, 10983−10989

Read Online

ACCESS | Metrics & More | Article Recommendations | Supporting Information

ABSTRACT: Tungsten diselenide (WSe_2) monolayers under strain are promising hosts for quantum emitters. To date, WSe_2 quantum emitter strain engineering has focused primarily on draping WSe_2 monolayers on patterned substrates and nanoindentation, which suffer from poor control over strain. In this work, we employ an electrostatic approach to dynamically control tensile strain in monolayer WSe_2 suspended over micron-scale cavities with a back gate contact. Room-temperature measurement of electrostatically induced deflection and photoluminescence at T = 100 K shows that a 0.22−0.26% increase in tensile strain can be achieved at modest gate voltages. Sharp localized emitters showed improvement in single photon purity from $g^{(2)}(0) = 0.55 \pm 0.04$ at 0 V to $g^{(2)}(0) = 0.40 \pm 0.05$ at −30 V due to strain-induced alignment of defect and dark exciton states and classical light background suppression.

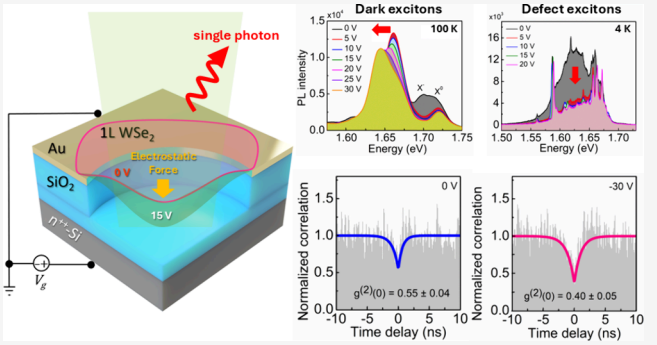

KEYWORDS: *strain engineering, two-dimensional materials, tungsten diselenide, single photon emitters, electrostatic biasing*

Semiconducting transition metal dichalcogenides (TMDs) are van der Waals materials consisting of transition metal atoms (Mo, W), each covalently bonded to two chalcogen atoms (S, Se, Te) to form a hexagonal crystal structure.[1−3] Two-dimensional (2D) semiconducting monolayer TMDs have direct bandgaps, which makes them promising in electronics and optoelectronics, including applications such as excitonic transistors,[4,5] photovoltaic devices,[6,7] and quantum emitters.[8−10] Monolayer tungsten diselenide (1L WSe_2) has been of particular interest as a host for quantum emitters due to its spin-forbidden dark exciton ground state,[11−13] which hybridizes with defect states under tensile strain[14−17] to give rise to bright single photon emitters.[18−20] Excitement in quantum information and communications has arisen from the discovery of WSe_2-based quantum emitters, which can be integrated with more conventional optoelectronic devices.[21−25]

Straining techniques for the creation of WSe_2-based quantum emitters have focused primarily on the formation of static tensile strain via the transfer of 1L WSe_2 to prefabricated nanopillars[26−28] or plasmonic nanoparticles[27,28] or creation of localized strain using atomic force microscopy (AFM) indentation techniques.[29,30] However, such structures are complex to scale and can be challenging to integrate into optoelectronic systems.[31,32] In addition, dynamically controllable strain can be essential in understanding the impact of strain on coupling and hybridization of dark excitons and localized defect excitons forming bright single photon emitters.[33] Studies of 1L WSe_2 membranes suspended over an air cavity with a back-gate bias voltage have shown that tensile strain results in the formation of hybridized states in which the CB minima in 1L WSe_2 are brought into energetic resonance with defect level states, giving rise to increased photoluminescence (PL) intensity.[17] However, sharp localized emitters formed as a result of energy alignment and coupling between dark excitons and sub-bandgap defect states were not observed even at strain values as high as 1% tensile strain, which were reached only at back-gate bias voltage magnitudes over 200 V.[17]

In this study, we have devised and implemented electrostatic straining of suspended 1L WSe_2, focusing on strain values (0.2−0.4% strain) sufficient for single photon emission, which are achievable at low gate bias voltages ($|V_g| \leq 30$ V) via small cavity diameters (1.65−2 μm), both of which should facilitate integration with future optoelectronic devices and systems. The application of a negative back-gate bias voltage and the corresponding creation of tensile strain in monolayer WSe_2 results in improved single photon purity through a

Received: May 15, 2025
Revised: June 13, 2025
Accepted: June 24, 2025
Published: June 30, 2025

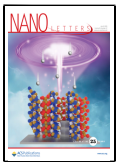

https://doi.org/10.1021/acs.nanolett.5c02619
Nano Lett. 2025, 25, 10983−10989

combination of classical light background reduction due to exciton dissociation,[30] carrier depletion,[34] and improved hybridization of the dark exciton and localized defect states.[15] We achieved an improvement in single photon purity from $g^{(2)}(0) = 0.55 \pm 0.04$ at $V_g = 0$ V to $g^{(2)}(0) = 0.40 \pm 0.05$ at $V_g = -30$ V, the latter clearly indicating single photon emission.

To create strain-tunable WSe_2 monolayers using electrostatic deflection, a monolayer of WSe_2 (1L WSe_2) is suspended over a substrate patterned with a hexagonal array of cavities (see Figure S1 for device fabrication process), with strain fields being generated by applying a bias voltage between the suspended 1L WSe_2 and a Si back gate. Here, the 1L WSe_2 is connected to a grounded top electrode (50 nm Au) and the bias voltage is applied to the bottom electrode (Si substrate), inducing an electrostatic attractive force between the two surfaces, which then results in the downward deflection of the 1L WSe_2 (see Figure 1a). Figure 1b shows an optical image of

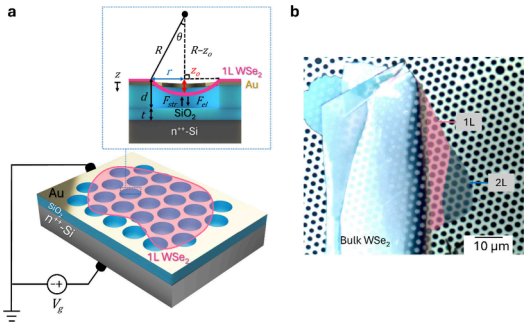

Figure 1. Monolayer WSe_2 (1L WSe_2) on cavity-patterned substrate and electrostatic straining approach. a) Schematic diagram of a 1L WSe_2 suspended over a substrate patterned with cavity arrays and the electrostatic straining approach. The inset shows the circumferential strain geometry of WSe_2 monolayer deflection over a single cavity. r: cavity radius, z_0: monolayer deflection, d: cavity depth, F_{str}: upward force due to strain, and F_{el}: downward force due to electrostatic interactions. b) Optical image of 1L WSe_2 suspended over cavity-patterned substrate.

1L WSe_2 suspended over a cavity-patterned substrate. Multiple cavities are covered with 1L (magenta area) and 2L (blue area) WSe_2, showing their clear suspension over the cavities.

To demonstrate the actual electrostatic deflection of a 1L WSe_2 membrane suspended over a cavity, bias voltages ranging from $V_g = 0$ to 15 V were applied to the Si back gate, and the corresponding monolayer deflection was measured using tapping mode AFM. All the experiments were carried out with air as the ambient at a temperature of $T = 298$ K. Figure 2a shows AFM topographic images of a 1L WSe_2 suspended over a patterned substrate measured at applied voltages $V_g = 0$, 5, 10, and 15 V. The 1L WSe_2 (enclosed by dashed black lines) experienced a clear and increasing downward deflection at applied bias voltages of $V_g = 10$ V and $V_g = 15$ V, as shown by the presence of depressed (dark blue) regions in the AFM topographic images (see Figure 2a). The height profiles corresponding to the deflection geometry of the suspended 1L WSe_2 at three different cavity sites are depicted in Figure 2b. When the applied voltage was increased initially from $V_g = 0$ V to $V_g = 5$ V, no significant monolayer deflection was observed. The absence of deflection at $V_g = 5$ V can be ascribed primarily to the air pressure build-up below the suspended monolayer WSe_2, suppressing the initial deflection of WSe_2. However, when the applied voltage was further increased to $V_g = 10$ V, an average deflection of 30 ± 12 nm was present. The monolayer reached an average deflection of 52 ± 9 nm at $V_g = 15$ V. Based on Equation S1, this corresponds to a $0.26 \pm 0.09\%$ increase in the tensile strain of the 1L WSe_2. Figure 2c shows the theoretical (magenta curve) and experimental (black circles) deflection of 1L WSe_2 suspended over a cavity deduced from the plots in Figure S2 and S3, confirming the good agreement between measured deflection as a function of bias voltage and that predicted by Equation S2. Note that an initial strain of ~ 0.2% at 0 V is present due to the initial 30–40 nm monolayer sagging (see Figure S4) before back-gate bias application.[35]

The application of uniform biaxial tensile strain to monolayer WSe_2 lowers the energy of the CB minima at the K and K' valleys in the Brillouin zone, yielding a redshift of exciton states of approximately 95 meV/% strain, which is typically observed in their PL emission spectra measured at $T = 100$ K.[17,36] Figures 3a and b show the photoluminescence (PL) intensity spectra and the corresponding PL intensity contour map as functions of energy and applied voltage (see Figure 3c) for the 1L WSe_2 suspended over a single cavity with the laser excitation spot centered on the cavity, measured at $T = 100$ K for both positive and negative bias voltages. Three major exciton emission peaks are observed, including neutral exciton (X^0) at 1.72 eV, charged trion (X^-) at 1.70 eV, and dark exciton (D^0) at 1.64–1.67 eV. These energy values agree well with the values reported in the literature for strained 1L WSe_2.[17,37,38] At $V_g = 0$ V, the negatively charged trion peak (X^-) was observed at 1.70 eV, as the 1L WSe_2 is almost charge neutral, with fluctuations in carrier density facilitating the transfer of excess electrons to WSe_2 at low temperatures.[39,40] Due to the small cavity dimensions used in this study, changes in strain and carrier concentration can occur simultaneously even at low bias voltages ($|V_g| \leq 30$ V). Therefore, when $|V_g| \geq 5$ V is applied to the silicon back gate, dark excitons (D^0) start to dominate the PL emission spectra while the trion peak (X^-) is suppressed at 0.02–0.22% tensile strain, suggesting that the strain effect is dominant in this voltage regime. The suppression of the X^- peak and the appearance of D^0 peak in this strain regime were also observed in previous reports[17] and can be attributed to the more effective funneling of dark excitons, which have longer lifetimes, to regions of localized strain as compared with charged trions.[11,41]

While the application of tensile strain through electrostatic biasing changes the band structure of 1L WSe_2, shifting the energy levels of both spin-allowed bright neutral excitons (X^0) and spin-forbidden dark excitons (D^0), dark excitons are more strongly influenced by changes in crystal lattice structure due to their strong phonon coupling through lattice vibrations, which results in a larger shift in their energy levels with strain.[42,43] Significant redshifts of the D^0 emission peak were observed at increasing applied voltages for both voltage polarities (see Figures 3a and b). We measured the D^0 energy shifts relative to the D^0 peak energy at $V_g = 0$ V as a function of applied voltage, as depicted in Figures 3d and e. When the applied voltage is increased from $V_g = 0$ V to $V_g = 30$ V, a 21 meV shift of the D^0 peak was observed, corresponding to a 0.22% increase in the tensile strain of 1L WSe_2. On the other hand, when the applied voltage is decreased from $V_g = 0$ V to $V_g = -30$ V, a 14 meV shift of the D^0 peak was observed, corresponding to a 0.15% increase in the tensile strain. Similar D^0 energy shifts were also observed at different cavity sites (see Figure S5).

https://doi.org/10.1021/acs.nanolett.5c02619
Nano Lett. 2025, 25, 10983–10989

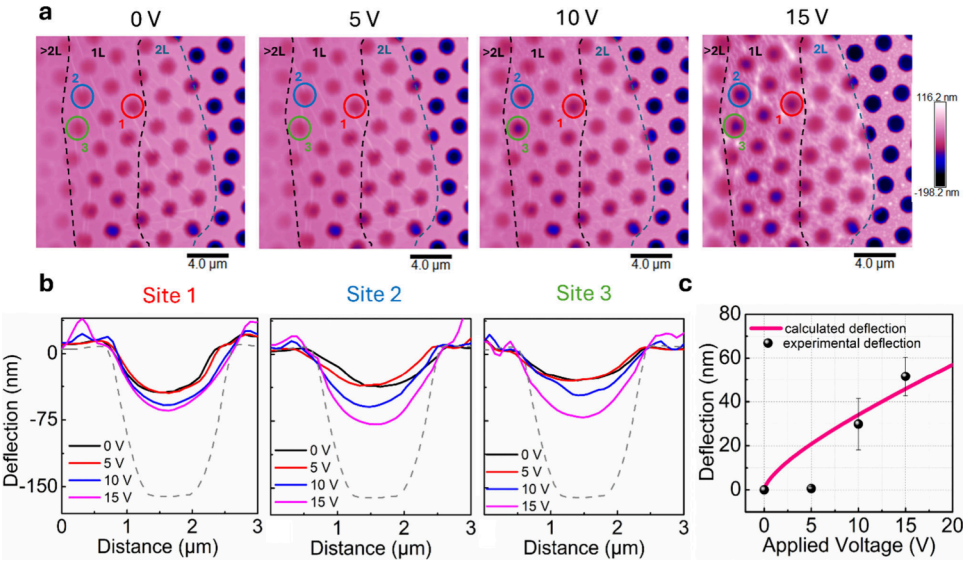

Figure 2. Electrostatic deflection of suspended 1L WSe_2 at room temperature (T = 298 K). a) AFM topographic images measured using tapping mode at different applied voltages: V_g = 0, 5, 10, and 15 V, showing monolayer deflection at increasing applied voltage. The 1L WSe_2 is enclosed in a dashed black curve, while the boundary region of 2L WSe_2 is indicated by a dashed blue curve. b) Height profiles of 1L WSe_2 at three different cavity sites, revealing significant deflection as the applied voltage increases. The dashed gray curve shows the cavity depth profile, showing a cavity depth of 170 nm. c) Comparison between calculated (magenta curve) and experimental (black circles) monolayer deflection, showing the monolayer starts deflecting between V_g = 5 and 10 V.

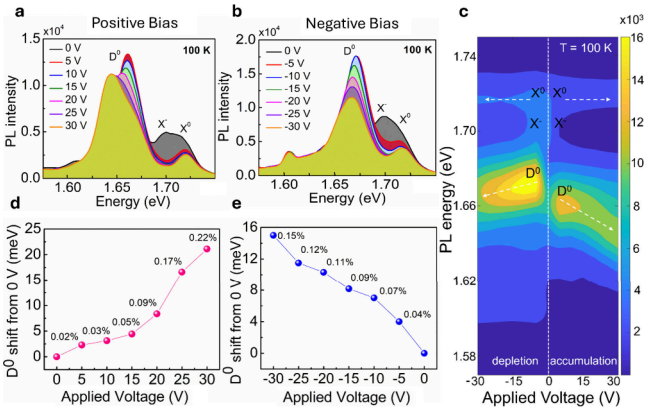

Figure 3. Control of dark excitons at T = 100 K. a, b) Photoluminescence (PL) intensity spectra as a function of applied voltage and the corresponding PL intensity contour map (c) of 1L WSe_2 suspended over a single cavity site measured at T = 100 K for different applied voltages: positive bias (a) and negative bias (b). Three major exciton emission peaks are observed − neutral exciton (X^0) at 1.72 eV, charged trion (X^-) at 1.70 eV, and dark exciton (D^0) at 1.64−167 eV. d, e) Measured dark exciton (D^0) energy shift relative to the D^0 peak energy at V_g = 0 V as the applied voltage is changed for both positive (d) and negative (e) voltage polarities. The estimated tensile strain value is indicated at each applied voltage, assuming a redshift of exciton states at 95 meV/% strain at T = 100 K and a 0% strain at V_g = 0 V.

We also observed a small asymmetry in the PL intensity at different voltage polarities, as illustrated in the PL intensity contour plot in Figure 3c, where electron accumulation (positive bias) and depletion (negative bias) are expected. This may arise due to the difference in the carrier density in WSe_2 for different voltage polarities, wherein a small oscillator strength difference of excitons is observed for n-doped (electron accumulation) WSe_2 monolayers.[44,45] Therefore, with the significant redshifts of D^0 emission peak energy as the tensile strain increases with the change in applied voltage for both polarities and evident changes in PL intensity between positive and negative applied voltages as a result of difference in carrier concentrations, we propose that significant changes in strain and carrier concentration can occur simultaneously even at low bias voltages ($|V_g| \leq 30$ V).

To understand the origin of localized emitters associated with single photon emission in strained 1L WSe_2, we examine the photoluminescence behavior of dark excitons and localized defect excitons at T = 4 K. For strained 1L WSe_2 under optical excitation, excitons are generated within the area of the excitation spot. Dark excitons, which have long diffusion lengths and recombination lifetimes, are coupled and hybridized with localized emitters that are in energetic resonance with sub-bandgap defect states under tensile strain, allowing the radiative recombination of localized defect excitons.[46] Figures 4a and b show the photoluminescence intensity spectra and corresponding contour map of PL intensity as functions of energy and applied voltage (see Figure 4c) for 1L WSe_2 suspended over a single cavity site measured at different applied voltages at T = 4 K. Several sharp localized emission peaks with linewidths of 0.9 to 1 meV, sufficiently narrow to be associated with single photon emission,[47,48] are clearly visible. When the applied voltage is changed from V_g = 0 V to V_g = ± 20 V in 5 V increments, the sharp localized emission peaks show minimal energy shift as the bias voltage magnitude and thus tensile strain increase, consistent with localized defect states in WSe_2 that are commonly unaffected by the strained lattice environment.[15,18] These sharp localized emission peaks are observed at two energies, 1.65−1.67 eV and 1.57−1.59 eV (white arrows in the contour map, labeled Defect 1 and Defect 2, respectively), corresponding to energies of defect states consisting of a single Se vacancy in monolayer WSe_2.[14,17] It is noteworthy that sharp localized emitters are observed even at V_g = 0 V due to the initial strain in the 1L WSe_2, which is estimated to be ∼ 0.2% tensile strain.

https://doi.org/10.1021/acs.nanolett.5c02619
Nano Lett. 2025, 25, 10983−10989

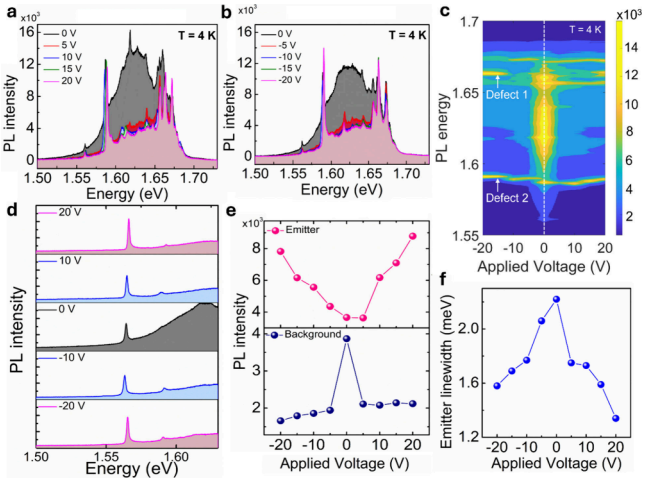

Figure 4. Sharp localized emitter peaks and classical light background suppression at T = 4 K. a, b) PL intensity spectra and (c) the corresponding PL intensity contour map of 1L WSe_2 suspended over a single cavity site measured at T = 4 K for different applied voltages: positive bias (a) and negative bias (b). d) PL intensity spectra of a single emitter on a different site measured at different applied voltages, showing a clear classical light background suppression at nonzero back-gate bias. e) Emitter peak intensity and background intensity of the chosen single emitter as a function of applied voltage. f) FWHM emitter linewidth of a single emitter as a function of applied voltage.

Since electrostatic gating simultaneously controls tensile strain and carrier behavior in 1L WSe_2, we observed pronounced suppression of the classical light background for both positive and negative voltages (see Figure S6). Figure 4d shows the photoluminescence intensity spectra of a single emitter on a different cavity site measured at different applied voltages, showing a significant 40 to 50% reduction in the classical light background, which overlaps in energy with the sharp localized emitters, as the applied voltage is changed from V_g = 0 V to V_g = ±20 V. This can be attributed to the dissociation of weakly bound exciton states, which typically contribute to a broad background of classical light that overlaps in energy with the localized emitters and thereby decreases the single photon purity.[30,49] At negative back-gate bias, a slightly stronger background suppression is observed due to carrier depletion. We also observed significant evidence of the formation of hybridized states, including single emitter intensity increase (see Figure 4e) and emitter linewidth decrease (see Figure 4f) as the applied voltage is changed in both voltage polarities. A two-fold increase in single emitter intensity was observed when the applied voltage was changed from V_g = 0 V to V_g = ± 20 V (see Figure 4e), which we attribute to the increase in tensile strain with applied voltage, which improves the energy alignment of the dark exciton ground state and localized defect states. It should be noted that the emitter intensity increase was calculated relative to the background intensity, and while most emitters showed an increase in emitter intensity at increasing tensile strain, spectral wandering,[31] intensity fluctuation,[31] and emitter blinking[50] are still observed in different sites (see Figure S6). Moreover, a decrease in FWHM emitter linewidth from 2.22 meV (V_g = 0 V) to 1.34 meV (V_g = 20 V) (see Figure 4f) was observed as the bias voltage was changed, which can be ascribed to the improved hybridization, wherein dark excitons occupy discrete defect energy levels, resulting in strong spatial confinement of localized excitons with highly localized emission spectra.[18] Combining these two phenomena with classical light background reduction due to exciton dissociation and carrier depletion as the applied voltage is changed can be beneficial for designing a pathway to improve the single photon purity of the localized emitters through an electrostatic straining approach.[30]

Finally, we demonstrate improvement of single photon purity as a result of classical light background suppression and improved energy alignment between dark excitons and localized defect excitons at increasing tensile strain induced by the applied back-gate bias voltage. Figure 5a shows the

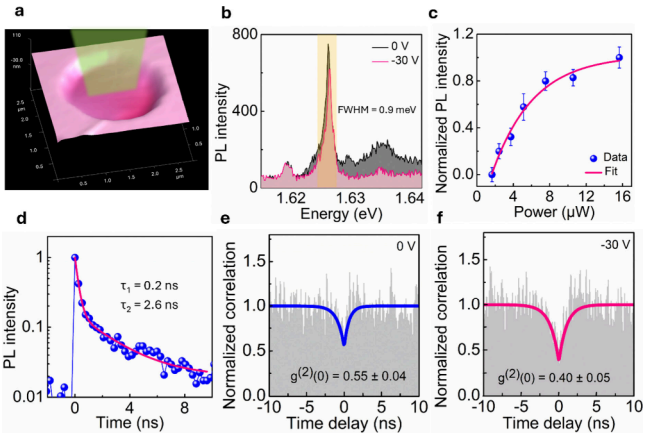

Figure 5. Improvement of single photon purity with applied bias voltage. a) 3D AFM topographic image of 1L WSe_2 on a single cavity. The green area denotes the laser excitation spot, illuminating 60−70% of the cavity. b) PL intensity spectra of a single emitter measured at V_g = 0 V and V_g = −30 V on a cavity site shown in (a). c) PL saturation behavior of a single emitter as a function of laser excitation power. d) PL lifetime of a single emitter. e) Second-order photon correlation at V_g = 0 V and V_g = −30 V (f), showing improvement in single photon purity. Note that the second-order correlation measurements are performed at T = 4 K, where the localized emitters show characteristics of single photon emitters (see Figure S7).

AFM topographic image of a WSe_2 monolayer suspended over a single cavity. The PL intensity spectra of a single isolated emitter are shown in Figure 5b, revealing a clear background reduction when the applied voltage is changed from V_g = 0 V to V_g = −30 V. As shown in Figure 4e, negative bias voltage, corresponding to the depletion of mobile electrons from the WSe_2 monolayer, yields stronger background suppression[34] and is therefore chosen for these measurements. Several key characteristics of single photon emitters are observed, including narrow emission peak linewidth (0.9 meV) (see Figure 5b), PL intensity saturation behavior at 5 μW excitation power (see Figure 5c), and a long component of emitter lifetime of τ_2 = 2.6 ns (see Figure 5d), all of which are consistent with the properties previously reported for single photon emitters based on strained 1L WSe_2.[47,48]

At V_g = 0 V, second-order photon correlation measurements yield $g^{(2)}(0) = 0.55 \pm 0.04$ (see Figure 5e), which is indicative of the presence of a low-purity single-photon emitter that is contaminated with a high classical light background. It should be noted that finding an isolated emitter with a good single photon purity, $g^{(2)}(0) < 0.5$, is often challenging due to the classical light background that overlaps in energy with the localized emitters.[14,15] When the applied voltage is changed to

https://doi.org/10.1021/acs.nanolett.5c02619
Nano Lett. 2025, 25, 10983−10989

V_g = −30 V, a $g^{(2)}(0)$ = 0.40 ± 0.05 was achieved (see Figure 5f), consistent with the observation of significant background suppression and improved intensity and linewidth for localized emission peaks for nonzero back-gate bias voltage, as shown in Figure 4. The improvement in antibunching behavior can be attributed to the classical light background suppression due to exciton dissociation and free carrier depletion, as well as the increase in tensile strain that improves the energy alignment of dark excitons and localized defect states. By applying a negative gate bias, charge depletion reduces the interaction between excitons and free carriers, which results in nonradiative decay suppression, improving the antibunching behavior of WSe_2-based quantum emitters.[34]

In summary, we have devised and characterized an electrostatic approach for dynamically controlling tensile strain in 1L WSe_2 suspended over micron-scale cavities with a silicon substrate acting as a back gate. Our results demonstrate (1) dynamic control of strain and dark exciton emission energy as the tensile strain increases with a change in applied back-gate voltage and (2) modulation of single photon emission through classical light background suppression and hybridization of dark exciton and localized defect states at nonzero back-gate bias, which combine to improve the antibunching behavior of single photon emitters. Changing the applied voltage from V_g = 0 V to V_g = −30 V improved the $g^{(2)}(0)$ value from 0.55 ± 0.04 to 0.40 ± 0.05, wherein the latter meets the accepted criterion for single photon emission of $g^{(2)}(0) < 0.5$.[29,47,48,51,52] This improvement in single photon purity is attributed to better hybridization with defect states, exciton dissociation, and carrier depletion at negative back-gate bias.[53] While exciton dissociation occurs for both voltage polarities, carrier depletion significantly improved the antibunching behavior. Although the purity of the observed single photon emitters from strained 1L WSe_2 on micron-scale cavities is thus inferior to that of nanopillars[26,54] or nanoindentations[55] due to a smaller strain gradient that promotes less efficient funneling of localized excitons,[56] our electrostatic straining approach can be implemented in nanoscale-sized cavities to create larger strain gradients and thereby, potentially yield higher-purity single photon emitters, offering outstanding potential toward more practical and scalable devices that can be readily integrated with various optoelectronic systems. When combined with precise defect engineering techniques,[14,15,18] the developed electrostatic straining approach could be a significant advance toward full control and manipulation of quantum emission based on strained 1L WSe_2. It can also be implemented toward the creation of dynamically controllable strain in other 2D materials such as monolayer hexagonal boron nitride (hBN), to investigate the nature and behavior of single photon emission at room temperature.[57,58] This can be beneficial in practical optoelectronic applications such as integrating 2D quantum emitters in optical cavities and waveguides.

METHODS

Detailed methods[59,60] are described in the Supporting Information.

ASSOCIATED CONTENT

Supporting Information

The Supporting Information is available free of charge at https://pubs.acs.org/doi/10.1021/acs.nanolett.5c02619.

Fabrication of cavity-patterned substrates; Modeling of electrostatically induced deflection of suspended 1L WSe_2; Derivation of strain using electrostatic deflection; Characterization of 1L WSe_2 suspended over cavity-patterned substrate; Optical measurements at low temperatures (T = 100 K and T = 4 K); Reproducibility of dark exciton energy shift at T = 100 K and classical light background suppression at T = 4 K; Temperature-dependent photoluminescence and second-order correlation (PDF)

AUTHOR INFORMATION

Corresponding Author

Edward T. Yu − *Chandra Family Department of Electrical and Computer Engineering, The University of Texas at Austin, Austin, Texas 78758, United States; Center for Dynamics and Control of Materials, The University of Texas at Austin, Austin, Texas 78758, United States*; Email: ety@ece.utexas.edu

Authors

Frances Camille M. Wu − *Chandra Family Department of Electrical and Computer Engineering, The University of Texas at Austin, Austin, Texas 78758, United States; Center for Dynamics and Control of Materials, The University of Texas at Austin, Austin, Texas 78758, United States;* orcid.org/0000-0002-8114-203X

Shang-Hsuan Wu − *Chandra Family Department of Electrical and Computer Engineering, The University of Texas at Austin, Austin, Texas 78758, United States;* orcid.org/0000-0001-9934-7765

Bin Fang − *Center for Dynamics and Control of Materials, The University of Texas at Austin, Austin, Texas 78758, United States*

Xintong Li − *Chandra Family Department of Electrical and Computer Engineering, The University of Texas at Austin, Austin, Texas 78758, United States; Center for Dynamics and Control of Materials, The University of Texas at Austin, Austin, Texas 78758, United States;* orcid.org/0000-0001-8566-0558

Jadon Zheng − *Chandra Family Department of Electrical and Computer Engineering, The University of Texas at Austin, Austin, Texas 78758, United States; Center for Dynamics and Control of Materials, The University of Texas at Austin, Austin, Texas 78758, United States*

Jean Anne C. Incorvia − *Chandra Family Department of Electrical and Computer Engineering, The University of Texas at Austin, Austin, Texas 78758, United States; Center for Dynamics and Control of Materials, The University of Texas at Austin, Austin, Texas 78758, United States;* orcid.org/0000-0002-4805-2112

Complete contact information is available at: https://pubs.acs.org/10.1021/acs.nanolett.5c02619

Author Contributions

F.C.M.W. performed the device fabrication, electrostatic biasing and AFM characterizations, photoluminescence measurements, second-order correlation measurements, and data analysis. S.-H.W. assisted in device fabrication, electrostatic biasing, and AFM characterizations. B.F., X. L., and J.A.C.I. assisted in the optical characterization and electrostatic biasing at cryogenic temperatures. J.Z. assisted in the device

https://doi.org/10.1021/acs.nanolett.5c02619
Nano Lett. 2025, 25, 10983−10989

fabrication and wire bonding. E.T.Y. assisted in project design and supervised the research. F.C.M.W. and E.T.Y. wrote the manuscript.

Funding

This work was primarily supported by the National Science Foundation through the Center for Dynamics and Control of Materials: an NSF MRSEC under Cooperative Agreement Nos. DMR-1720595 and DMR-2308817. Additional support was provided by NSF under Grant Nos. DMR-1905287 and DMR-2413468. The authors acknowledge the use of facilities and instrumentation supported by the National Science Foundation through the Center for Dynamics and Control of Materials: an NSF MRSEC under Cooperative Agreement Nos. DMR-1720595 and DMR-2308817. This work was performed in part at the University of Texas Microelectronics Research Center, a member of the National Nanotechnology Coordinated Infrastructure (NNCI), which is supported by the National Science Foundation (grant ECCS-2025227).

Notes

The authors declare no competing financial interest.

■ ACKNOWLEDGMENTS

The authors acknowledge the contribution of Professor Daniel Wasserman and Yadviga Tischenko in the wire bonding experiments for device fabrication.

■ ABBREVIATIONS

1L WSe_2, monolayer tungsten diselenide; 2L WSe_2, bilayer tungsten diselenide; r, cavity radius; z_0, monolayer deflection; d, cavity depth; F_{str}, upward force due to strain; F_{el}, downward force due to electrostatic forces; V_g, gate voltage

■ REFERENCES

(1) Clark, G.; Schaibley, J. R.; Ross, J.; Taniguchi, T.; Watanabe, K.; Hendrickson, J. R.; Mou, S.; Yao, W.; Xu, X. Single Defect Light-Emitting Diode in a van der Waals Heterostructure. *Nano Lett.* **2016**, *16* (6), 3944−3948.

(2) Koperski, M.; Nogajewski, K.; Arora, A.; Cherkez, V.; Mallet, P.; Veuillen, J. Y.; Marcus, J.; Kossacki, P.; Potemski, M. Single photon emitters in exfoliated WSe_2 structures. *Nat. Nanotechnol.* **2015**, *10* (6), 503−506.

(3) Michaelis de Vasconcellos, S.; Wigger, D.; Wurstbauer, U.; Holleitner, A. W.; Bratschitsch, R.; Kuhn, T. Single-Photon Emitters in Layered van der Waals Materials. *physica status solidi (b)* **2022**, *259* (4), 2100566.

(4) Withers, F.; Del Pozo-Zamudio, O.; Schwarz, S.; Dufferwiel, S.; Walker, P. M.; Godde, T.; Rooney, A. P.; Gholinia, A.; Woods, C. R.; Blake, P.; Haigh, S. J.; Watanabe, K.; Taniguchi, T.; Aleiner, I. L.; Geim, A. K.; Fal'ko, V. I.; Tartakovskii, A. I.; Novoselov, K. S. WSe_2 Light-Emitting Tunneling Transistors with Enhanced Brightness at Room Temperature. *Nano Lett.* **2015**, *15* (12), 8223−8228.

(5) Seyler, K. L.; Schaibley, J. R.; Gong, P.; Rivera, P.; Jones, A. M.; Wu, S.; Yan, J.; Mandrus, D. G.; Yao, W.; Xu, X. Electrical control of second-harmonic generation in a WSe_2 monolayer transistor. *Nat. Nanotechnol.* **2015**, *10* (5), 407−411.

(6) Kim, K.-H.; Andreev, M.; Choi, S.; Shim, J.; Ahn, H.; Lynch, J.; Lee, T.; Lee, J.; Nazif, K. N.; Kumar, A.; Kumar, P.; Choo, H.; Jariwala, D.; Saraswat, K. C.; Park, J.-H. High-Efficiency WSe_2 Photovoltaic Devices with Electron-Selective Contacts. *ACS Nano* **2022**, *16* (6), 8827−8836.

(7) Tang, Y.; Wang, Z.; Wang, P.; Wu, F.; Wang, Y.; Chen, Y.; Wang, H.; Peng, M.; Shan, C.; Zhu, Z.; Qin, S.; Hu, W. WSe_2 Photovoltaic Device Based on Intramolecular p-n Junction. *Small* **2019**, *15* (12), 1805545.

(8) Kumar, S.; Kaczmarczyk, A.; Gerardot, B. D. Strain-Induced Spatial and Spectral Isolation of Quantum Emitters in Mono- and Bilayer WSe_2. *Nano Lett.* **2015**, *15* (11), 7567−7573.

(9) He, Y.-M.; Clark, G.; Schaibley, J. R.; He, Y.; Chen, M.-C.; Wei, Y.-J.; Ding, X.; Zhang, Q.; Yao, W.; Xu, X.; Lu, C.-Y.; Pan, J.-W. Single quantum emitters in monolayer semiconductors. *Nat. Nanotechnol.* **2015**, *10* (6), 497−502.

(10) Chen, X.; Lu, X.; Dubey, S.; Yao, Q.; Liu, S.; Wang, X.; Xiong, Q.; Zhang, L.; Srivastava, A. Entanglement of single-photons and chiral phonons in atomically thin WSe_2. *Nat. Phys.* **2019**, *15* (3), 221−227.

(11) Gelly, R. J.; Renaud, D.; Liao, X.; Pingault, B.; Bogdanovic, S.; Scuri, G.; Watanabe, K.; Taniguchi, T.; Urbaszek, B.; Park, H.; Lončar, M. Probing dark exciton navigation through a local strain landscape in a WSe_2 monolayer. *Nat. Commun.* **2022**, *13* (1), 232.

(12) Branny, A.; Kumar, S.; Proux, R.; Gerardot, B. D. Deterministic strain-induced arrays of quantum emitters in a two-dimensional semiconductor. *Nat. Commun.* **2017**, *8* (1), 15053.

(13) Li, X.; Wang, W.; Ma, X. Quantum Photon Sources in WSe_2 Monolayers Induced by Weakly Localized Strain Fields. *J. Phys. Chem. C* **2022**, *126* (47), 20057−20064.

(14) Utama, M. I. B.; Zeng, H.; Sadhukhan, T.; Dasgupta, A.; Gavin, S. C.; Ananth, R.; Lebedev, D.; Wang, W.; Chen, J.-S.; Watanabe, K.; Taniguchi, T.; Marks, T. J.; Ma, X.; Weiss, E. A.; Schatz, G. C.; Stern, N. P.; Hersam, M. C. Chemomechanical modification of quantum emission in monolayer WSe_2. *Nat. Commun.* **2023**, *14* (1), 2193.

(15) Xu, D. D.; Vong, A. F.; Lebedev, D.; Ananth, R.; Wong, A. M.; Brown, P. T.; Hersam, M. C.; Mirkin, C. A.; Weiss, E. A. Conversion of Classical Light Emission from a Nanoparticle-Strained WSe_2 Monolayer into Quantum Light Emission via Electron Beam Irradiation. *Adv. Mater.* **2023**, *35* (5), 2208066.

(16) Ye, Y.; Dou, X.; Ding, K.; Chen, Y.; Jiang, D.; Yang, F.; Sun, B. Single photon emission from deep-level defects in monolayer WSe_2. *Phys. Rev. B* **2017**, *95* (24), 245313.

(17) Hernández López, P.; Heeg, S.; Schattauer, C.; Kovalchuk, S.; Kumar, A.; Bock, D. J.; Kirchhof, J. N.; Höfer, B.; Greben, K.; Yagodkin, D.; Linhart, L.; Libisch, F.; Bolotin, K. I. Strain control of hybridization between dark and localized excitons in a 2D semiconductor. *Nat. Commun.* **2022**, *13* (1), 7691.

(18) Parto, K.; Azzam, S. I.; Banerjee, K.; Moody, G. Defect and strain engineering of monolayer WSe_2 enables site-controlled single-photon emission up to 150 K. *Nat. Commun.* **2021**, *12* (1), 3585.

(19) Dang, J.; Sun, S.; Xie, X.; Yu, Y.; Peng, K.; Qian, C.; Wu, S.; Song, F.; Yang, J.; Xiao, S.; Yang, L.; Wang, Y.; Rafiq, M. A.; Wang, C.; Xu, X. Identifying defect-related quantum emitters in monolayer WSe_2. *npj 2D Materials and Applications* **2020**, *4* (1), 2.

(20) Linhart, L.; Paur, M.; Smejkal, V.; Burgdörfer, J.; Mueller, T.; Libisch, F. Localized Intervalley Defect Excitons as Single-Photon Emitters in WSe_2. *Phys. Rev. Lett.* **2019**, *123* (14), 146401.

(21) Peyskens, F.; Chakraborty, C.; Muneeb, M.; Van Thourhout, D.; Englund, D. Integration of single photon emitters in 2D layered materials with a silicon nitride photonic chip. *Nat. Commun.* **2019**, *10* (1), 4435.

(22) Errando-Herranz, C.; Schöll, E.; Picard, R.; Laini, M.; Gyger, S.; Elshaari, A. W.; Branny, A.; Wennberg, U.; Barbat, S.; Renaud, T.; Sartison, M.; Brotons-Gisbert, M.; Bonato, C.; Gerardot, B. D.; Zwiller, V.; Jöns, K. D. Resonance Fluorescence from Waveguide-Coupled, Strain-Localized, Two-Dimensional Quantum Emitters. *ACS Photonics* **2021**, *8* (4), 1069−1076.

(23) Blauth, M.; Jürgensen, M.; Vest, G.; Hartwig, O.; Prechtl, M.; Cerne, J.; Finley, J. J.; Kaniber, M. Coupling Single Photons from Discrete Quantum Emitters in WSe_2 to Lithographically Defined Plasmonic Slot Waveguides. *Nano Lett.* **2018**, *18* (11), 6812−6819.

(24) Gao, T.; von Helversen, M.; Antón-Solanas, C.; Schneider, C.; Heindel, T. Atomically-thin single-photon sources for quantum communication. *npj 2D Materials and Applications* **2023**, *7* (1), 4.

(25) Moody, G.; Tran, K.; Lu, X.; Autry, T.; Fraser, J. M.; Mirin, R. P.; Yang, L.; Li, X.; Silverman, K. L. Microsecond Valley Lifetime of

Defect-Bound Excitons in Monolayer WSe_2. *Phys. Rev. Lett.* **2018**, *121* (5), 057403.
(26) Cai, T.; Kim, J.-H.; Yang, Z.; Dutta, S.; Aghaeimeibodi, S.; Waks, E. Radiative Enhancement of Single Quantum Emitters in WSe_2 Monolayers Using Site-Controlled Metallic Nanopillars. *ACS Photonics* **2018**, *5* (9), 3466−3471.
(27) Tripathi, L. N.; Iff, O.; Betzold, S.; Dusanowski, Ł.; Emmerling, M.; Moon, K.; Lee, Y. J.; Kwon, S.-H.; Höfling, S.; Schneider, C. Spontaneous Emission Enhancement in Strain-Induced WSe_2 Monolayer-Based Quantum Light Sources on Metallic Surfaces. *ACS Photonics* **2018**, *5* (5), 1919−1926.
(28) Guo, S.; Germanis, S.; Taniguchi, T.; Watanabe, K.; Withers, F.; Luxmoore, I. J. Electrically Driven Site-Controlled Single Photon Source. *ACS Photonics* **2023**, *10* (8), 2549−2555.
(29) So, J.-P.; Kim, H.-R.; Baek, H.; Jeong, K.-Y.; Lee, H.-C.; Huh, W.; Kim, Y. S.; Watanabe, K.; Taniguchi, T.; Kim, J.; Lee, C.-H.; Park, H.-G. Electrically driven strain-induced deterministic single-photon emitters in a van der Waals heterostructure. *Science Advances* **2021**, *7* (43), eabj3176.
(30) Stevens, C. E.; Chuang, H.-J.; Rosenberger, M. R.; McCreary, K. M.; Dass, C. K.; Jonker, B. T.; Hendrickson, J. R. Enhancing the Purity of Deterministically Placed Quantum Emitters in Monolayer WSe_2. *ACS Nano* **2022**, *16* (12), 20956−20963.
(31) Srivastava, A.; Sidler, M.; Allain, A. V.; Lembke, D. S.; Kis, A.; Imamoğlu, A. Optically active quantum dots in monolayer WSe_2. *Nat. Nanotechnol.* **2015**, *10* (6), 491−496.
(32) Kern, J.; Niehues, I.; Tonndorf, P.; Schmidt, R.; Wigger, D.; Schneider, R.; Stiehm, T.; Michaelis de Vasconcellos, S.; Reiter, D. E.; Kuhn, T.; Bratschitsch, R. Nanoscale Positioning of Single-Photon Emitters in Atomically Thin WSe_2. *Adv. Mater.* **2016**, *28* (33), 7101−7105.
(33) Chakraborty, C.; Jungwirth, N. R.; Fuchs, G. D.; Vamivakas, A. N. Electrical manipulation of the fine-structure splitting of WSe_2 quantum emitters. *Phys. Rev. B* **2019**, *99* (4), 045308.
(34) Cai, H.; Rasmita, A.; He, R.; Zhang, Z.; Tan, Q.; Chen, D.; Wang, N.; Mu, Z.; Eng, J. J. H.; She, Y.; Pan, N.; Wang, Q.; Dong, Z.; Wang, X.; Wang, J.; Miao, Y.; Singh, R.; Qiu, C.-W.; Liu, X.; Gao, W. Charge-depletion-enhanced WSe_2 quantum emitters on gold nanogap arrays with near-unity quantum efficiency. *Nat. Photonics* **2024**, *18* (8), 842−847.
(35) Huang, J.; Hoang, T. B.; Mikkelsen, M. H. Probing the origin of excitonic states in monolayer WSe_2. *Sci. Rep.* **2016**, *6* (1), 22414.
(36) Peng, Z.; Chen, X.; Fan, Y.; Srolovitz, D. J.; Lei, D. Strain engineering of 2D semiconductors and graphene: from strain fields to band-structure tuning and photonic applications. *Light: Science & Applications* **2020**, *9* (1), 190.
(37) Kim, G.; Kim, H. M.; Kumar, P.; Rahaman, M.; Stevens, C. E.; Jeon, J.; Jo, K.; Kim, K.-H.; Trainor, N.; Zhu, H.; Sohn, B.-H.; Stach, E. A.; Hendrickson, J. R.; Glavin, N. R.; Suh, J.; Redwing, J. M.; Jariwala, D. High-Density, Localized Quantum Emitters in Strained 2D Semiconductors. *ACS Nano* **2022**, *16* (6), 9651−9659.
(38) Chen, Z.-Z.; Chang, C.-Y.; Tsai, Y.-T.; Tsai, P.-C.; Lin, S.-Y.; Shih, M.-H. Sustained robust exciton emission in suspended monolayer WSe_2 within the low carrier density regime for quantum emitter applications. *APL Materials* **2024**, *12* (3), 031125.
(39) Lyons, T. P.; Dufferwiel, S.; Brooks, M.; Withers, F.; Taniguchi, T.; Watanabe, K.; Novoselov, K. S.; Burkard, G.; Tartakovskii, A. I. The valley Zeeman effect in inter- and intra-valley trions in monolayer WSe_2. *Nat. Commun.* **2019**, *10* (1), 2330.
(40) Wang, Z.; Liu, Y.; Chen, D.; Wang, Z.; Asbahi, M.; Rezaei, S. D.; Deng, J.; Teng, J.; Wee, A. T. S.; Zhang, W.; Yang, J. K. W.; Dong, Z. Nanocavity-induced trion emission from atomically thin WSe_2. *Sci. Rep.* **2022**, *12* (1), 15861.
(41) Lv, Y.; Abid, M.; Cheng, H. H.; Coileáin, C. Ó.; Sofin, R. G. S.; Chang, C.-R.; Wu, H.-C. Strain-Dependent Optical Properties of Monolayer WSe_2. *J. Phys. Chem. C* **2023**, *127* (46), 22682−22691.
(42) Feierabend, M.; Khatibi, Z.; Berghäuser, G.; Malic, E. Dark exciton based strain sensing in tungsten-based transition metal dichalcogenides. *Phys. Rev. B* **2019**, *99* (19), 195454.
(43) Mueller, T.; Malic, E. Exciton physics and device application of two-dimensional transition metal dichalcogenide semiconductors. *npj 2D Materials and Applications* **2018**, *2* (1), 29.
(44) Shinokita, K.; Wang, X.; Miyauchi, Y.; Watanabe, K.; Taniguchi, T.; Matsuda, K. Continuous Control and Enhancement of Excitonic Valley Polarization in Monolayer WSe_2 by Electrostatic Doping. *Adv. Funct. Mater.* **2019**, *29* (26), 1900260.
(45) Allain, A.; Kis, A. Electron and Hole Mobilities in Single-Layer WSe_2. *ACS Nano* **2014**, *8* (7), 7180−7185.
(46) Sortino, L.; Zotev, P. G.; Phillips, C. L.; Brash, A. J.; Cambiasso, J.; Marensi, E.; Fox, A. M.; Maier, S. A.; Sapienza, R.; Tartakovskii, A. I. Bright single photon emitters with enhanced quantum efficiency in a two-dimensional semiconductor coupled with dielectric nano-antennas. *Nat. Commun.* **2021**, *12* (1), 6063.
(47) Ripin, A.; Peng, R.; Zhang, X.; Chakravarthi, S.; He, M.; Xu, X.; Fu, K.-M.; Cao, T.; Li, M. Tunable phononic coupling in excitonic quantum emitters. *Nat. Nanotechnol.* **2023**, *18* (9), 1020−1026.
(48) Li, X.; Jones, A. C.; Choi, J.; Zhao, H.; Chandrasekaran, V.; Pettes, M. T.; Piryatinski, A.; Tschudin, M. A.; Reiser, P.; Broadway, D. A.; Maletinsky, P.; Sinitsyn, N.; Crooker, S. A.; Htoon, H. Proximity-induced chiral quantum light generation in strain-engineered $WSe_2/NiPS_3$ heterostructures. *Nat. Mater.* **2023**, *22* (11), 1311−1316.
(49) Massicotte, M.; Vialla, F.; Schmidt, P.; Lundeberg, M. B.; Latini, S.; Haastrup, S.; Danovich, M.; Davydovskaya, D.; Watanabe, K.; Taniguchi, T.; Fal'ko, V. I.; Thygesen, K. S.; Pedersen, T. G.; Koppens, F. H. L. Dissociation of two-dimensional excitons in monolayer WSe_2. *Nat. Commun.* **2018**, *9* (1), 1633.
(50) He, Y.-M.; Iff, O.; Lundt, N.; Baumann, V.; Davanco, M.; Srinivasan, K.; Höfling, S.; Schneider, C. Cascaded emission of single photons from the biexciton in monolayered WSe_2. *Nat. Commun.* **2016**, *7* (1), 13409.
(51) Paralikis, A.; Piccinini, C.; Madigawa, A. A.; Metuh, P.; Vannucci, L.; Gregersen, N.; Munkhbat, B. Tailoring polarization in WSe_2 quantum emitters through deterministic strain engineering. *npj 2D Materials and Applications* **2024**, *8* (1), 59.
(52) Michler, P.; Imamoğlu, A.; Mason, M. D.; Carson, P. J.; Strouse, G. F.; Buratto, S. K. Quantum correlation among photons from a single quantum dot at room temperature. *Nature* **2000**, *406* (6799), 968−970.
(53) Xu, D. D.; Vong, A. F.; Utama, M. I. B.; Lebedev, D.; Ananth, R.; Hersam, M. C.; Weiss, E. A.; Mirkin, C. A. Sub-Diffraction Correlation of Quantum Emitters and Local Strain Fields in Strain-Engineered WSe_2 Monolayers. *Adv. Mater.* **2024**, *36* (25), 2314242.
(54) Palacios-Berraquero, C.; Kara, D. M.; Montblanch, A. R. P.; Barbone, M.; Latawiec, P.; Yoon, D.; Ott, A. K.; Loncar, M.; Ferrari, A. C.; Atatüre, M. Large-scale quantum-emitter arrays in atomically thin semiconductors. *Nat. Commun.* **2017**, *8* (1), 15093.
(55) Abramov, A. N.; Chestnov, I. Y.; Alimova, E. S.; Ivanova, T.; Mukhin, I. S.; Krizhanovskii, D. N.; Shelykh, I. A.; Iorsh, I. V.; Kravtsov, V. Photoluminescence imaging of single photon emitters within nanoscale strain profiles in monolayer WSe_2. *Nat. Commun.* **2023**, *14* (1), 5737.
(56) Lee, H.; Koo, Y.; Choi, J.; Kumar, S.; Lee, H.-T.; Ji, G.; Choi, S. H.; Kang, M.; Kim, K. K.; Park, H.-R.; Choo, H.; Park, K.-D. Drift-dominant exciton funneling and trion conversion in 2D semiconductors on the nanogap. *Science Advances* **2022**, *8* (5), eabm5236.
(57) Aharonovich, I.; Tetienne, J.-P.; Toth, M. Quantum Emitters in Hexagonal Boron Nitride. *Nano Lett.* **2022**, *22* (23), 9227−9235.
(58) Tran, T. T.; Bray, K.; Ford, M. J.; Toth, M.; Aharonovich, I. Quantum emission from hexagonal boron nitride monolayers. *Nat. Nanotechnol.* **2016**, *11* (1), 37−41.
(59) Wu, S.-H.; Cossio, G.; Braun, B.; Wu, F. C. M.; Yu, E. T. Smart Window Structures Based on Highly Conductive, Transparent Metal Nanomeshes and Thermochromic Perovskite Films. *Advanced Optical Materials* **2023**, *11* (6), 2202409.
(60) Cossio, G.; Yu, E. T. Zeta Potential Dependent Self-Assembly for Very Large Area Nanosphere Lithography. *Nano Lett.* **2020**, *20* (7), 5090−5096.

https://doi.org/10.1021/acs.nanolett.5c02619
Nano Lett. 2025, 25, 10983−10989